

Memory Gym: Towards Endless Tasks to Benchmark Memory Capabilities of Agents

Marco Pleines

*Department of Computer Science
TU Dortmund University
Dortmund, 44227, Germany*

MARCO.PLEINES@TU-DORTMUND.DE

Matthias Pallasch

*Department of Computer Science
TU Dortmund University
Dortmund, 44227, Germany*

MATTHIAS.PALLASCH@TU-DORTMUND.DE

Frank Zimmer

*Department of Communication and Environment
Rhine-Waal University of Applied Sciences
Kamp-Lintfort, 47475, Germany*

FRANK.ZIMMER@HOCHSCHULE-RHEIN-WAAL.DE

Mike Preuss

*Leiden Institute of Advanced Computer Science
Universiteit Leiden
EZ Leiden, 2311, The Netherlands*

M.PREUSS@LIACS.LEIDENUNIV.NL

Editor: My editor

Abstract

Memory Gym presents a suite of 2D partially observable environments, namely Mortar Mayhem, Mystery Path, and Searing Spotlights, designed to benchmark memory capabilities in decision-making agents. These environments, originally with finite tasks, are expanded into innovative, endless formats, mirroring the escalating challenges of cumulative memory games such as “I packed my bag”. This progression in task design shifts the focus from merely assessing sample efficiency to also probing the levels of memory effectiveness in dynamic, prolonged scenarios. To address the gap in available memory-based Deep Reinforcement Learning baselines, we introduce an implementation that integrates Transformer-XL (TrXL) with Proximal Policy Optimization. This approach utilizes TrXL as a form of episodic memory, employing a sliding window technique. Our comparative study between the Gated Recurrent Unit (GRU) and TrXL reveals varied performances across different settings. TrXL, on the finite environments, demonstrates superior sample efficiency in Mystery Path and outperforms in Mortar Mayhem. However, GRU is more efficient on Searing Spotlights. Most notably, in all endless tasks, GRU makes a remarkable resurgence, consistently outperforming TrXL by significant margins.

Website and Source Code: <https://github.com/MarcoMeter/endless-memory-gym/>

Keywords: deep reinforcement learning, proximal policy optimization, memory, transformer, recurrence

1 Introduction

Imagine embarking on a long-awaited family vacation, with the open road stretching ahead. As the car hums along, a lively atmosphere envelops the passengers, young and old alike, as they engage in a playful game of “I packed my bag”. Each family member takes turns adding an item to an imaginary bag, attempting to remember and recite the growing list correctly. However, as the game unfolds and the list lengthens, the passengers encounter mounting challenges illustrating the finite nature of their individual memories. Despite best efforts, varying strategies, and different capabilities, the weight of the growing list eventually leads to resignation.

Memory is not just a game – it is a critical tool for intelligent decision-making under imperfect information and uncertainty. Without the ability to recall past experiences, reasoning, creativity, planning, and learning may become elusive. In the realm of autonomously learning decision-making agents as Deep Reinforcement Learning (DRL), the agent’s memory involves maintaining a representation of previous observations, a knowledge bank that grounds its next decision. Memory mechanisms, be it through recurrent neural networks (Rumelhart et al., 1986) or transformers (Vaswani et al., 2017), have enabled these agents to master tasks both virtual and real. For instance, DRL methods have conquered complex video games as Capture the flag (Jaderberg et al., 2018), StarCraft II (Vinyals et al., 2019), and DotA 2 (Berner et al., 2019). Their success extends beyond virtual environments to real-world challenges as dexterous in-hand manipulation (Andrychowicz et al., 2020) and controlling tokamak plasmas (Degrave et al., 2022).

1.1 Endless Tasks Benchmark Memory Effectiveness and not just Efficiency

Cumulative memory games, such as “I packed my bag”, introduce an automatic curriculum through their inherently progressive and unbounded nature. The game’s expansion depends on the participants’ continuous success. Exploiting the concept of ‘endlessness’ in tasks can provide deeper insights into the effectiveness of decision-makers when facing escalating demands of memory retention and recall. Such challenges inevitably test the limits of an agent’s memory. Here, ‘effectiveness’ refers to the ability to attain higher scores, indicative of more powerful memory capabilities. Contrasting this, traditional DRL memory benchmarks are centered around sample efficiency, influenced by the defined boundaries and fixed goals of finite tasks, which do not accommodate perpetual tasks.

1.2 Contributions: Novel Memory Benchmark and Transformer-XL Baseline

In our prior research, we introduced Memory Gym (Pleines et al., 2023), an open-source benchmark, designed to challenge memory-based DRL agents to memorize events across long sequences, generalize, be robust to noise, and be sample efficient. Memory Gym encompasses three distinct finite environments: Mortar Mayhem, Mystery Path, and Searing Spotlights. Each environment presents visual observations, multi-discrete action spaces, and crucially, they cannot be mastered without memory, demanding frequent memory interactions. Building on this foundation, we advance Memory Gym by evolving each environment into an endless format, inspired by the “I packed my bag” game, to further test and de-

velop memory capabilities in DRL agents. To our current understanding, no existing DRL memory benchmark possesses such endless tasks.

We further contribute an open-source and easy-to-follow baseline implementation of Transformer-XL (TrXL) (Dai et al., 2019) based on the widely-used DRL algorithm Proximal Policy Optimization (PPO) (Schulman et al., 2017). A recurring theme in the realm of memory-based DRL is the lack of accessible and reproducible baselines. Many significant works, particularly those utilizing transformers (Fortunato et al., 2019; Parisotto et al., 2020; Hill et al., 2021; Lampinen et al., 2021; Parisotto and Salakhutdinov, 2021), have not made their implementations publicly available. As implementation details of DRL algorithms are vital (Engstrom et al., 2020; Andrychowicz et al., 2021; Huang et al., 2022b), this lack of transparency poses significant challenges for the research community, hindering progress and reproducibility. Therefore, our accessible implementation can serve as a beacon for the community fostering further research.

In our experimental analysis, we benchmark a TrXL and a recurrent agent, based on the Gated Recurrent Unit (GRU) (Cho et al., 2014), across the original (finite) and the new endless environments of Memory Gym. Our findings indicate that TrXL performs best in terms of sample efficiency on Mystery Path and effectiveness on Mortar Mayhem. However, in the Searing Spotlights environment, GRU demonstrates better sample efficiency. To our greatest surprise, in the endless environments, GRU consistently surpasses TrXL in effectiveness by large margins.

1.3 Overview

This paper begins with related work, followed by illustrating the dynamics in Memory Gym’s environments, particularly focusing on their endless formats. We detail the actor-critic model architecture, including the loss functions and key elements of the TrXL baseline. The subsequent section presents our experimental analysis, showcasing results from both finite and endless tasks. We further explore TrXL’s underperformance in endless tasks, providing insights and suggestions for future research. Before concluding, we falsify our initial hypothesis about recurrence’s vulnerability to spotlight perturbations in Searing Spotlights, emphasizing the significant impact of not normalizing estimated advantages during agent optimization.

2 Related Work

Previous studies have explored the use of memory-based agents in a variety of tasks. Some of them are originally fully observable but are turned into partially observable Markov Decision Processes by adding noise or masking out information from the agent’s observation space (Hausknecht and Stone, 2015; Heess et al., 2015; Meng et al., 2021; Shang et al., 2021). Subsequently we give a coarse overview of recently used benchmarks chronologically.

Deepmind Lab 30 (Beattie et al., 2016) presents a collection of 30 procedurally generated first-person 3D environments. Starting from a general motor-control navigation task and visual observations, each environment poses a different goal such as collecting fruit, playing laser tag or traversing a maze. Pašukonis et al. (2023) have identified that agents can exploit the environments’ skyboxes, which reduces the demands on memory.

Minigrid (Chevalier-Boisvert et al., 2018) includes a 2D grid memory task inspired by the T-Maze (Wierstra et al., 2007). In this environment, the agent is required to memorize an initial goal cue, traverse a long alley, and correctly choose the exit once the end is reached.

Miniworld (Chevalier-Boisvert, 2018) encompasses a set of first-person 3D environments based on the tasks introduced by Minigrid.

VizDoom (Wydmuch et al., 2018) features first-person shooter 3D environments that revolve around motor-control navigation tasks, with the added challenge of computer-controlled enemies that may confront the agent.

The **Memory Task Suite** (Fortunato et al., 2019) includes diverse memory-based environments across four categories: PsychLab (Leibo et al., 2018) for image-based tasks (e.g. detect change), Spot the Difference for cue memorization, goal navigation tasks inspired by the Morris water maze (D’Hooge and De Deyn, 2001), and transitive object ordering tasks.

Progen (Cobbe et al., 2020) consists of 16 2D environments that offer procedurally generated and fully observable levels. These environments encompass a combination of puzzle-solving, platforming, and action-based games. 6 of these environments have been modified to become partially observable by reducing and centering the agent’s visual observation.

Numpad (Parisotto et al., 2020) requires the agent to accurately press a series of keys in a specific sequence of fixed length. The sequence itself is not provided to the agent, resulting in the agent employing a trial-and-error approach while memorizing the underlying sequence.

Memory Maze (Parisotto et al., 2020) shares similarities with the Morris Water maze (D’Hooge and De Deyn, 2001), as the agent must locate an apple, then undergoes random repositioning, requiring it to find the apple’s location again and again.

Dancing the Ballet (Ballet) (Lampinen et al., 2021) presents a sequence of up to 8 dances visually, with the agent remaining stationary. After all the dances are displayed, the agent is required to identify a specific one to successfully complete the task.

PopGym (Morad et al., 2023), published at ICLR 2023 alongside Memory Gym (Pleines et al., 2023), is a benchmark with 15 environments classified as diagnostic, control, noisy, game, or navigation. These are designed for rapid convergence, offering vector instead of visual observations.

Memory Maze (Pašukonis et al., 2023) showcases procedurally generated 3D mazes, where agents, from a first-person perspective, are tasked with locating specific objects as requested by the environment. Additionally, the authors have collected a dataset tailored for offline reinforcement learning.

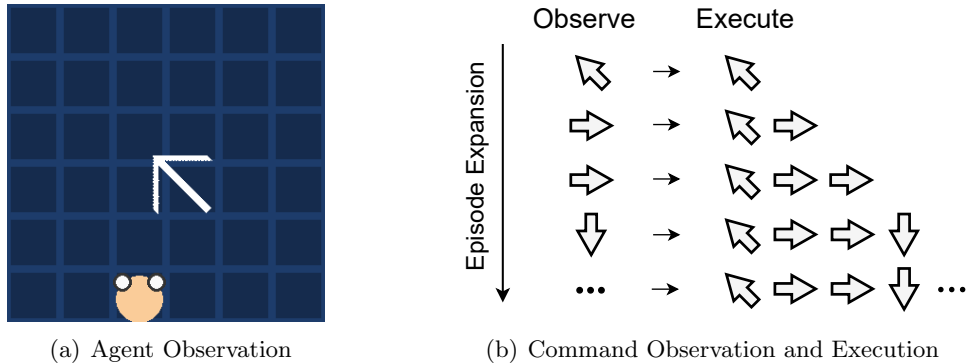


Figure 1: Endless Mortar Mayhem (a) is observed from a top-down view and its arena occupies the entire screen. If the agent, depicted as a circle with white paws, walks off, it re-enters from the opposite side. Episodes endlessly expand by alternately visualizing and executing commands (b), behaving as an automatic curriculum.

Memory Gym’s environments offer a unique feature that sets them apart from the aforementioned benchmarks: an endless design tailored to rigorously test memory capabilities. It is important to clarify that ‘endless’ should not be confused with ‘open-ended’. Memory Gym’s endless environments are not open-ended in nature; they possess clear objectives and defined structures. In contrast, open-ended environments offer agents freedom to develop unique skills and strategies without stringent constraints as demonstrated by the Paired Open-Ended Trailblazer algorithm (Wang et al., 2020) or platforms like Minecraft (Fan et al., 2022).

3 Endless Memory Tasks Inspired by “I Packed My Bag”

Prior to the underlying work, we introduced Memory Gym, a set of finite tasks benchmarking agents to strongly depend on frequent memory interactions (Pleines et al., 2023). Memory Gym consists of the environments Mortar Mayhem, Mystery Path, and Searing Spotlights. All of them expose visual observations, capturing an area of, 84×84 RGB pixels, to the agent and allow for multi-discrete actions. Importantly, the original environments pose a single (or finite) goal. In this section, we delve into the intricacies of extrapolating the originally finite tasks to endless ones. Annex A presents the reset parameters to configure and scale the environments.

3.1 Endless Mortar Mayhem

The finite variant of Mortar Mayhem takes place inside a grid-like arena and comprises two tasks. Initially, the agent is immobile and must memorize a sequence of ten commands, followed by executing each command in the observed order. A command instructs the agent to move to an adjacent floor tile or remain at the current one. Failure to execute a command results in episode termination, whereas each successful execution yields a reward of +0.1.

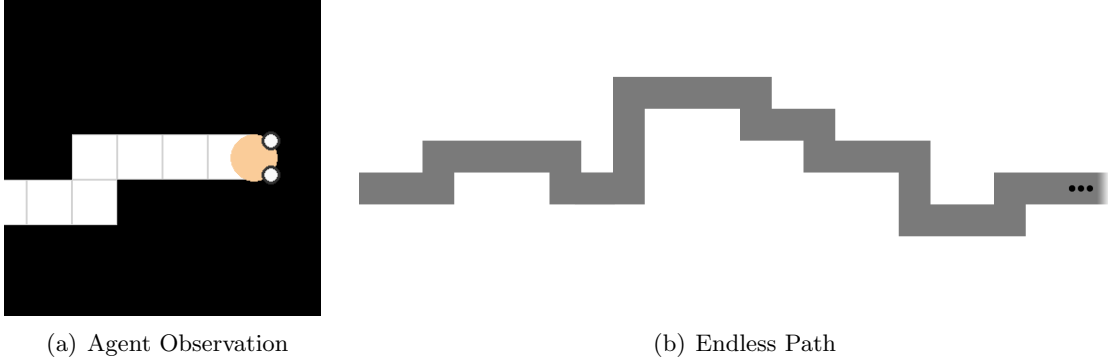


Figure 2: In Endless Mystery Path (a), the agent observes only a segment of the environment at a time. By rendering the path tiles past it, the agent acquires a sense of horizontal movement, even though its horizontal position remains visually constant. Figure (b) showcases an example of a procedurally generated endless path.

Endless Mortar Mayhem (Figure 1) extends the to-be-executed command sequence continuously, enabling potentially infinite sequences. To accommodate this, the command visualization and execution are alternated. As shown in Figure 1(b), an episode begins by displaying one command, followed by its execution. Subsequently, the next visualization reveals only the second command, requiring the agent to execute both the first and second commands. This automatic curriculum allows the to-be-executed command sequence to continually expand, while each new command is presented only once.

3.2 Endless Mystery Path

The core concept of the original Mystery Path environment requires the agent to navigate an invisible path until reaching its end. If the agent strays off the path, it is relocated to the path’s origin. To succeed, the agent must consistently memorize and recall its steps along the path, as well as the locations where it fell off.

Endless Mystery Path (Figure 2) introduces a never-ending path, which is always generated from left to right. Consequently, we eliminate the agent’s ability to move left. As the endless path cannot be fully captured in an 84×84 RGB pixel observation, we visually fix the agent’s horizontal position. If nothing but the agent is shown in the observation, the agent lacks information about its horizontal motion. To address this, we render the path tiles behind the agent, providing visual cues of the local horizontal position.

Regarding terminal conditions, we aim to shorten episodes if the agent performs poorly. Firstly, the agent is given a time budget of 20 steps to reach the next tile. This budget is reset when the agent moves to the next tile or falls off. Another condition terminates the episode if the agent falls off before reaching its best progress. Lastly, the episode is terminated if the agent falls off at the same location for a second time. With these conditions in place, an episode can potentially last indefinitely if the agent consistently succeeds.

In terms of rewards, the agent earns $+0.1$ for each previously unvisited tile of the path it reaches. While this may initially appear as a dense reward function, any misstep that

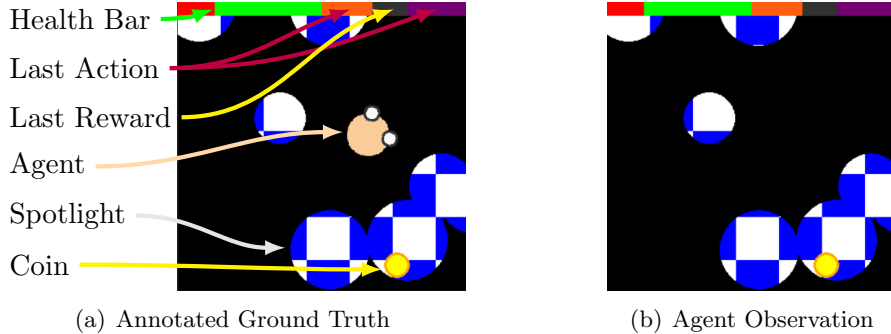


Figure 3: In Endless Searing Spotlights’ annotated ground truth, the top rows of pixels display the agent’s remaining health points, its last action, and indicate whether a positive reward was received during the last step. The last action is encoded using two chunks and three colors, while the last positive reward is represented by two colors. In the agent’s observation (b), the spotlights play a role in revealing or hiding other entities.

causes the agent to fall off means it cannot reclaim those rewards. The agent must retrace its steps and regain its prior progress to continue accumulating rewards. The longer it takes to catch up, the sparser the rewards become.

3.3 Endless Searing Spotlights

Endless Searing Spotlights (Figure 3) features a pitch-black environment illuminated only by moving and threatening spotlights. The agent starts with ten health points, losing one each time it is hit by a spotlight. At the beginning of each episode, the environment is fully lit, but it quickly dims to darkness within a few steps. The episode ends if the agent’s health points are depleted. To survive, the agent must cleverly use the darkness as cover, relying on memory to remember past actions and previous positions to infer its current location. The agent’s observation space includes its last action, current health, and any positive reward received in the previous step.

To mitigate monotonous behaviors, a coin collection task is incorporated. In the finite version, the agent aims to collect a randomly placed coin, worth $+0.25$, and then exit the level for an additional $+1$ reward. Effective memory use enables the agent to track its location, coin positions, and the exit. In the endless concept, the exit is removed, and the coin collection mechanism is revamped to spawn a new coin each time one is collected. This coin remains visible for six frames, while the agent has 160 steps to collect it. Distinct from the finite version, spotlights now appear at a steady rate, rather than intensifying over time.

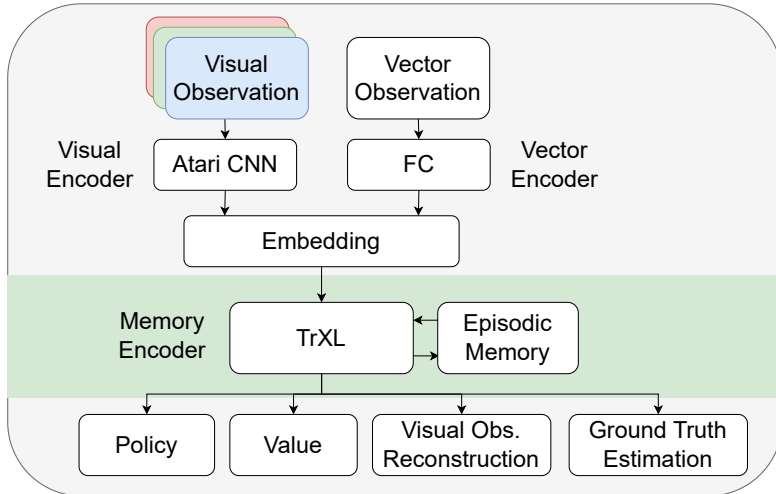


Figure 4: Overview of the actor-critic model architecture. The model features observation encoders and a memory encoder (green). The encoders’ parameters are shared among several heads dedicated to the policy, state-value function, observation reconstruction, and ground truth estimation.

4 Transformer-XL Baseline

In our experiments, we employ the widely-recognized Deep Reinforcement Learning (DRL) algorithm Proximal Policy Optimization (PPO) (Schulman et al., 2017). To add memory abilities to PPO, either recurrent neural networks (RNN) or attention mechanisms (i.e. transformer) are potential solutions. Prior works have extensively demonstrated the effectiveness of leveraging RNNs, such as Long Short-Term Memory (LSTM) (Hochreiter and Schmidhuber, 1997) and Gated Recurrent Unit (GRU) (Cho et al., 2014), within the realm of DRL (Mnih et al., 2016; Espeholt et al., 2018; Huang et al., 2022a). This also applies to previous studies employing transformers, as Gated Transformer-XL (GTrXL) (Parisotto et al., 2020) and Hierarchical Chunk Attention Memory (HCAM) (Lampinen et al., 2021). However, integrating these memory-enhancing techniques into DRL algorithms is not straightforward, particularly due to the dearth of readily available transformer-based DRL implementations. To bridge this gap, we contribute an easy-to-follow baseline implementation of Transformer-XL (TrXL) (Dai et al., 2019) in PPO. Before delving into the transformer-based PPO baseline, we describe the actor-critic model architecture and the losses used during training.

4.1 Actor-Critic Model Architecture

Figure 4 presents a broad overview of the actor-critic model architecture. The encoding process begins with visual observations, and optionally, vector observations (i.e. game state information). To encode visual observations (i.e. pixel observations) of shape $84 \times 84 \times 3$, we employ the Atari CNN (Mnih et al., 2015). The vector observation is encoded by a fully connected layer (FC). The outputs of these encoders are concatenated and subsequently

embedded into the input space of the transformer-based memory encoder. Once the data is propagated through the memory encoder, it is further processed by each individual head that may contain further fully connected hidden layers. The policy head (actor) samples multi-discrete actions as required by Memory Gym, while the value head (critic) approximates the state-value.

Optionally, there is a head dedicated to reconstructing the original visual observation to strengthen the learning signal: the latent output of the memory encoder is fed to a transposed Atari CNN. The utility of such an auxiliary head is demonstrated by some of our results (Section 5) and prior works by Lampinen et al. (2021) and Hill et al. (2021). During development, we also tried to attach the reconstruction head directly to the encoder, but this led to catastrophic results. Another optional head establishes a diagnosis tool by estimating ground truth information, which is provided as labels by the environment. Inspired by Baker et al. (2020), the parameters of this head can be optimized post agent training to assess whether distinct information can be queried from the agent’s memory.

4.2 Loss Function Composition

Our baseline utilizes PPO’s clipped surrogate objective (Schulman et al., 2017). Due to leveraging memory, the to be selected action a_t of the policy π_θ depends on the current observation o_t and the memory encoder’s output that we refer to as hidden state h_t .

$$L_t^C(\theta) = -\mathbb{E}_t [\min (q_t(\theta) A_\pi^{\text{GAE}}(o_t, h_t, a_t), \text{clip}(q_t(\theta), 1 - \epsilon, 1 + \epsilon) A_\pi^{\text{GAE}}(o_t, h_t, a_t))] \quad (1)$$

$$\text{with ratio } q_t(\theta) = \frac{\pi(a_t|o_t, h_t, \theta)}{\pi(a_t|o_t, h_t, \theta_{\text{old}})}$$

A_π^{GAE} denotes advantage estimates based on generalized advantage estimation (GAE) (Schulman et al., 2016), θ the trainable parameters of a neural net, and ϵ the clip range. t depicts the current time step. The value function is optimized using the clipped squared-error loss $L_t^V(\theta)$, which is apparent in the implementation of Schulman et al. (2017):

$$L_t^{VClip}(\theta) = \left(\text{clip}(V(o_t, h_t, \theta), V(o_t, h_t, \theta_{\text{old}}) - \epsilon, V(o_t, h_t, \theta_{\text{old}}) + \epsilon) - \hat{V} \right)^2 \quad (2)$$

$$L_t^V(\theta) = \max \left[\left(V(o_t, h_t, \theta) - \hat{V} \right)^2, L_t^{VClip}(\theta) \right] \quad (3)$$

The auxiliary observation reconstruction is optimized using the binary cross entropy:

$$L_t^R(o_t, \hat{o}_t) = -[\hat{o}_t \log(o_t) + (1 - \hat{o}_t) \log(1 - o_t)], \quad (4)$$

and the optional ground truth estimation leverages the squared-error loss, which optimizes the concerned head’s parameters ϕ :

$$L_t^Y(\hat{y}_t, y_t, \phi) = (\hat{y}_t - y_t)^2 \quad (5)$$

The final combined loss is depicted by $L_t^{C+V+H+R+Y}(\theta)$:

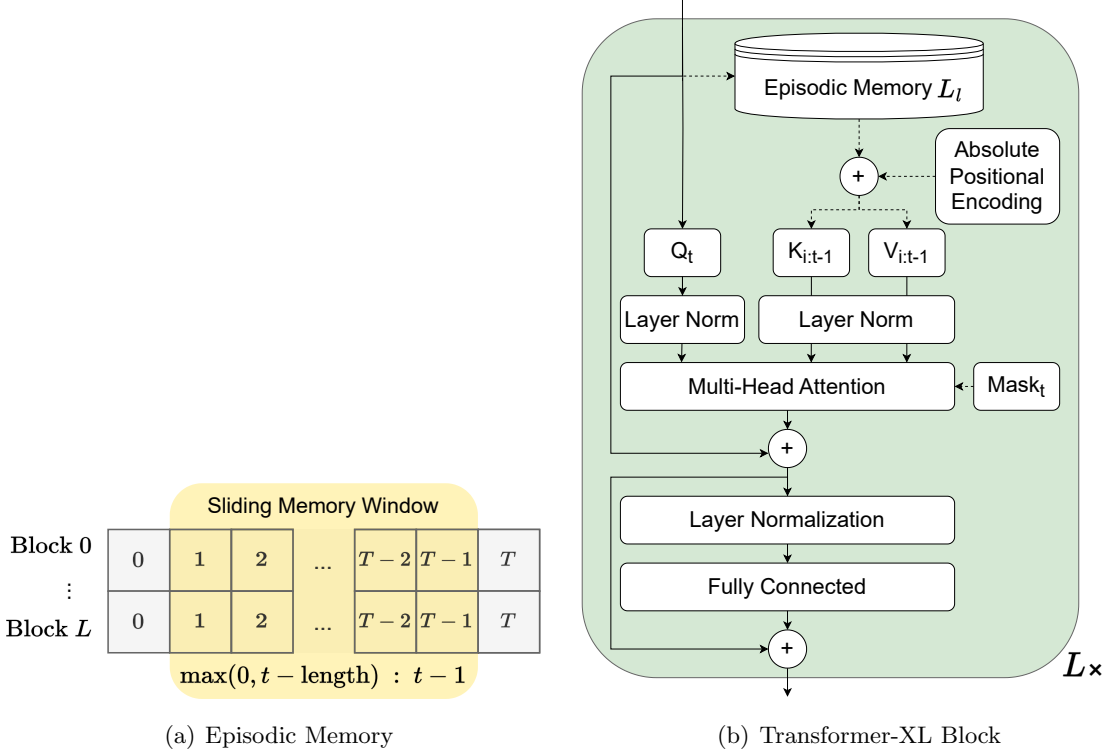


Figure 5: Figure (a) illustrates the episodic memory that stores past inputs to all Transformer-XL blocks for every step taken by the agent. Input sequences to the Transformer-XL blocks are retrieved using a sliding memory window. T denotes the episode length. Figure (b) depicts the architecture of one Transformer-XL block that is stacked L times. The dashed lines state that there is no gradient flow into the episodic memory, the absolute positional encoding, and the mask.

$$L_t^{C+V+H+R+Y}(\theta) = \mathbb{E}_t[L_t^C(\theta) + c_1 L_t^V(\theta) - c_2 \mathcal{H}[\pi_\theta](o_t, h_t) + c_3 L_t^R(o_t, \hat{o}_t) + c_4 L_t^Y(\theta)] \quad (6)$$

where $\mathcal{H}[\pi_\theta](o_t, h_t)$ denotes an entropy bonus encouraging exploration (Schulman et al., 2017). c_1 to c_4 are coefficients to scale each loss, excluding the clipped surrogate objective.

4.3 Transformer-XL as Memory Mechanism

When processing sequential data, transformers employ attention mechanisms to capture global dependencies in parallel across the entire sequence (Vaswani et al., 2017), while RNNs iteratively propagate information through recurrent connections. Our transformer baseline draws conceptual inspiration from TrXL (Dai et al., 2019), GTrXL (Parisotto et al., 2020), and HCAM (Lampinen et al., 2021). The original transformer architecture proposed by

Vaswani et al. (2017) is designed as a sequence-to-sequence model with an encoder-decoder structure. However, for the purpose of DRL, we adapt the architecture to a sequence-to-one model, focusing solely on the encoder as done in GTrXL and HCAM. This modification is driven by the underlying Markov Decision Process, which maps the environment’s current state to a single action rather than a sequence of actions.

To begin with, it needs to be clarified what kind of sequential data is fed to a transformer, which is typically composed of multiple stacked blocks. Naively, the input data can be conceptualized as a sequence of observations. In the context of visual observations, this is commonly referred to as frame stacking, where consecutive frames are combined. However, instead of expensively stacking raw frames, we leverage the past outputs of the model’s embedding module (Figure 4), which serves as the input sequence to the first transformer block. The subsequent blocks make use of the past outputs from their preceding blocks. These sequences, those elements we refer to as hidden states, are stored in the agent’s episodic memory (Figure 5(a)) and are collected during inference based on the episode’s current timestep t . To accommodate computational challenges of potentially endless episodes, we employ a sliding memory window approach, where the input sequence of past hidden states is derived from a fixed-length window. By leveraging formerly computed hidden states in the input sequence, the agent’s memory facilitates the ability to attend to events that extend beyond the boundaries of the fixed-length memory window, aligning with the segment-level recurrence of TrXL (Dai et al., 2019). Note that gradients are not back propagated through the episodic memory. Once propagated through all transformer blocks, a final hidden state is produced to inform the agent’s policy.

The architecture of our TrXL encoder block is depicted in Figure 5(b). At each timestep t , the block receives an input that is solely based on the current timestep. This input is added to the episodic memory and serves as the query Q_t during the execution of multi-head attention (MHA) (Vaswani et al., 2017). The keys K and values V used in MHA are derived from the same data based on self-attention. Specifically, we retrieve K and V by slicing the episodic memory using the bounding indices $i = \max(0, t - \text{window length})$ and $t - 1$. To ensure the positional information of K and V remains coherent, we add a positional encoding following the approach from Vaswani et al. (2017). We use the absolute variant as a default as we found a learned one to be effective, but less sample efficient. The underlying positional encoding matrix is scaled to the maximum episode length and not to the length of the window. Therefore, every sequence element of an episode is associate with its distinct position. In the case of endless episodes, the length of the positional encoding is fixed to 2048.

To restrict attention to time steps up to the current timestep t , we employ a strictly lower triangular matrix as a mask in MHA. This mask is only necessary when t is smaller than the length of the sliding memory window. The remaining configuration of the block adheres to the findings of Parisotto et al. (2020), which suggest improved performance with pre layer normalization and the identity map reordering. We encountered vanishing gradient issues when applying layer normalization after MHA and the fully connected layer, which is referred to as post layer normalization. Although our implementation supports the gating mechanism of GTrXL, it resulted in either lower or equivalent performance while being computationally more expensive (Appendix C).

5 Experimental Analysis

We run empirical experiments on Memory Gym using the just introduced TrXL baseline and one based on GRU, both powered by Proximal Policy Optimization (Schulman et al., 2017). Contrary to our previous study (Pleines et al., 2023), we exclude HELM (History comprEsson via Language Models) (Paischer et al., 2022a) and its successor, HELMv2 (Paischer et al., 2022b). The decision stems from HELM’s suboptimal wall-time efficiency, which is six times more expensive than a GRU agent (Pleines et al., 2023), making hyperparameter optimization impractical for our purposes. As we are strongly limited by our compute budget of 25,000 GPU hours, we rather dedicated the resources towards the development of the endless environments and the TrXL baseline. We also conduct preliminary tests using Gated Transformer-XL (GTrXL) (Parisotto et al., 2020) and Long Short-Term Memory (LSTM) (Hochreiter and Schmidhuber, 1997) on the finite environments without any extensive hyperparameter tuning. These models usually underperformed when applied directly, suggesting that out-of-the-box applications might necessitate hyperparameter optimization.

As part of our evaluation protocol, the following sample efficiency curves depict the interquartile mean (IQM) along with a stratified bootstrapped confidence interval of 0.95 (shaded area on the plots), following the guidelines of Agarwal et al. (2021). Each training run is repeated 5 times. To evaluate the generalization ability of our baselines, we extensively test them on 50 novel environment seeds that were excluded from the training process. This evaluation is repeated 3 times for each data point, resulting in a comprehensive assessment based on a total of 750 episodes for every data point presented.

The next subsection presents a two-fold examination of the finite environments. Firstly, we reaffirm that memory is imperative in simpler environment instances, a conclusion previously drawn in our earlier study (Pleines et al., 2023). Enhanced hyperparameters allow us to report improved results. Secondly, we compare the performance of GRU and TrXL on the original finite tasks. TrXL exhibits stronger policies in Mortar Mayhem than GRU, while it is more sample efficient in Mystery Path. Searing Spotlights is an exception to this where TrXL is less sample efficient. Contradicting our initial expectations and the results on the finite environments, we unveil surprising findings that highlight GRU’s superiority over TrXL in all endless environments. For a comprehensive overview of the hyperparameters employed in our experiments, see Appendix B. Results for GTrXL and LSTM on the finite environments can be found in Appendix C. Additionally, a selection of wall-time efficiency statistics is available in Appendix D.

5.1 Finite Environments: Transformer-XL is often more efficient than GRU

Before assessing GRU and TrXL on the default challenges of the finite environments, the first set of experiments focuses on confirming that the agents trained on Memory Gym indeed require memory. To accomplish this, we train several minor baselines alongside GRU and TrXL on simplified versions of the environments. These baselines include PPO without memory, PPO with frame stacking (4 and 16 grayscale frames), and PPO with absolute positional encoding (Vaswani et al., 2017) provided as vector observation.

Results on Mortar Mayhem (Figures 6(a)-(c)) show the number of commands that were properly executed during one episode. In Mortar Mayhem Act Grid, where the commands

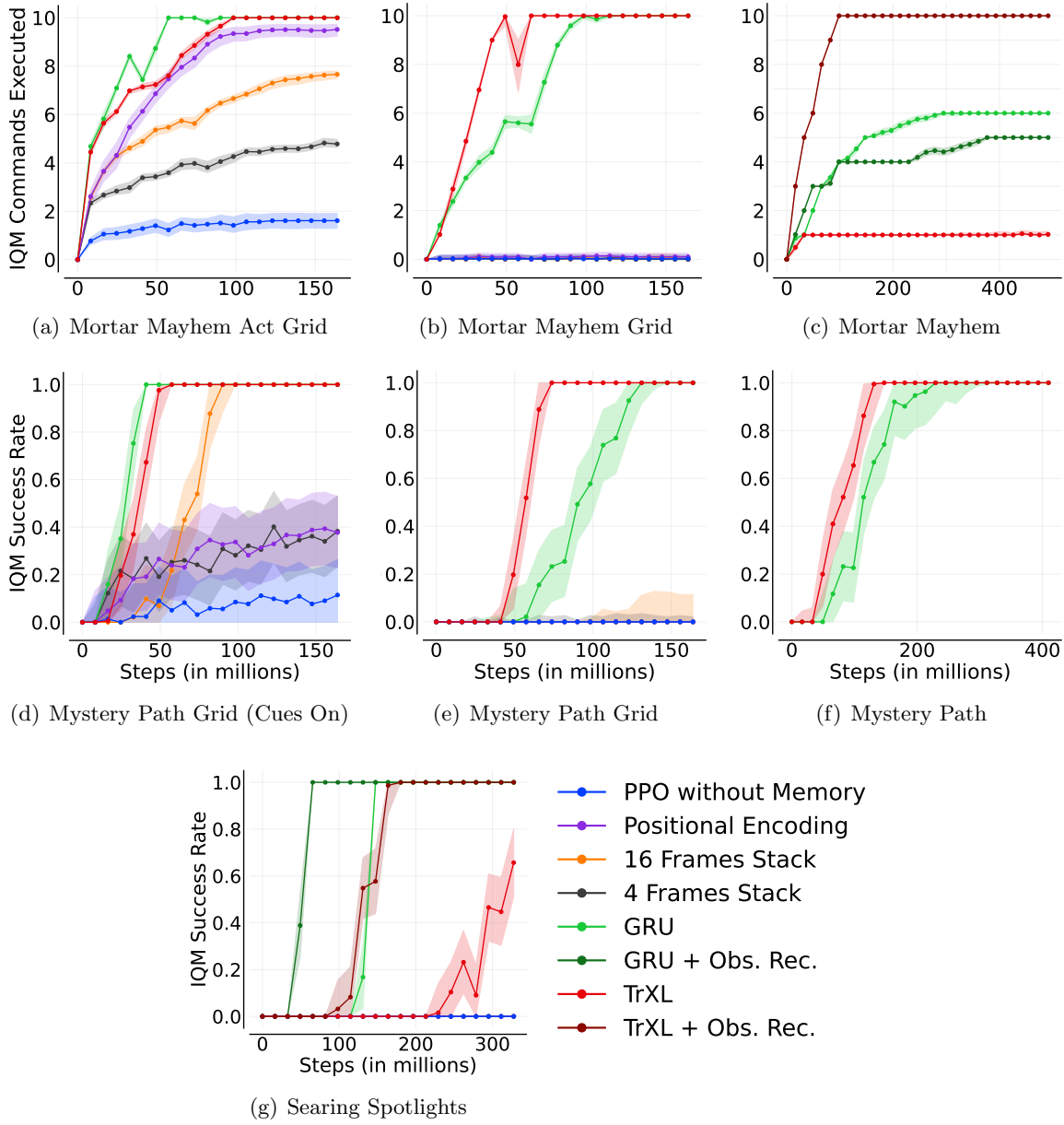


Figure 6: Performance comparison across instances of Memory Gym’s finite environments. Mortar Mayhem Act Grid (a) provides commands as a fully observable vector, bypassing the Clue Task. Both (a) and Mortar Mayhem Grid (b) utilize grid-like locomotion. (c) represents the default Mortar Mayhem task. Mystery Path Grid operates on grid-like locomotion, with (a) rendering the the goal and origin to the agent’s observation. (b) and (c) hide these, while (c) is the default Mystery Path task. Searing Spotlights (g) is not varied, while all conducted runs leverage observation reconstruction (Obs. Rec.) in this environment.

are completely provided as vector observation, PPO without memory is ineffective, while the frame stacking agents achieve nearly either 5 or 8 commands with a slight upward trend. Agents using GRU or TrXL are the most effective, completing all 10 commands, while the one with absolute positional encoding follows closely, completing 9.5 commands. The positional encoding baseline adds the episode’s current time step to the agent’s observation allowing for temporal awareness within the sequential execution of commands. Once the complete task is present (Figure 6(b)), only GRU and TrXL prove to be effective and therefore we conclude that Mortar Mayhem demands memory.

We obtain a similar impression when training on Mystery Path Grid where the origin and goal are not perceivable by the agent (Figure 6(e)). In this case, TrXL outperforms GRU in terms of sample efficiency, while both methods are effective. If the origin and the goal are visible, a horizon of 16 frames is sufficient to train an effective policy as shown by the frame stacking agent (Figure 6(d)). Stacking 4 frames or leveraging positional encoding leads to an IQM success rate of 40% with a slight trend upward. The memory-less agent’s success rate goes up to about 11%.

No success is proven by the minor baselines in Searing Spotlights as seen in Figure 6(g). Only in this experiment, the minor baselines also leverage observation reconstruction. Utilizing the observation reconstruction loss significantly improves the sample efficiency of GRU and TrXL. The reason for this can be found in rare events: the agent, the coin, and the exit are seldomly visible. Hence, the visual encoder takes advantage from the auxiliary learning signal provided by the observation reconstruction. However, both GRU variants, with and without observation reconstruction, exhibit notably higher sample efficiency compared to their respective TrXL counterparts.

When facing the default task of Mortar Mayhem, a different result becomes apparent (Figure 6(c)). TrXL with observation reconstruction solves all 10 commands after training for about 100 million steps, while GRU converges to only about 6 commands. GRU’s performance drops to about 5 commands if the observation reconstruction loss is used. If TrXL trains without this auxiliary loss, its performance drops to about only one successful command.

In the case of Mystery Path (Figure 6(f)), we opted not to train agents using observation reconstruction, as the always visible agent is the only entity that requires visual encoding. In this scenario, TrXL achieves the desired success rate in approximately 100 million steps, whereas GRU requires twice as many steps to achieve the same level of performance. If wall-time efficiency is compared, however, TrXL and GRU are roughly on par (Annex D).

In summary, TrXL proves to be more effective than GRU in Mortar Mayhem and exhibits higher sample efficiency in the case of Mystery Path. However, it is worth noting that GRU, both with and without observation reconstruction, outperforms its respective TrXL counterparts in Searing Spotlights.

5.2 Endless Environments: GRU is more effective than Transformer-XL

To our surprise, across all three endless environments, the recurrent agent consistently outperforms the transformer-based agent by a significant margin. This diverges from the observations made by Parisotto et al. (2020) and Lampinen et al. (2021), where an LSTM was found to be less effective. Notably, the most substantial performance gap between

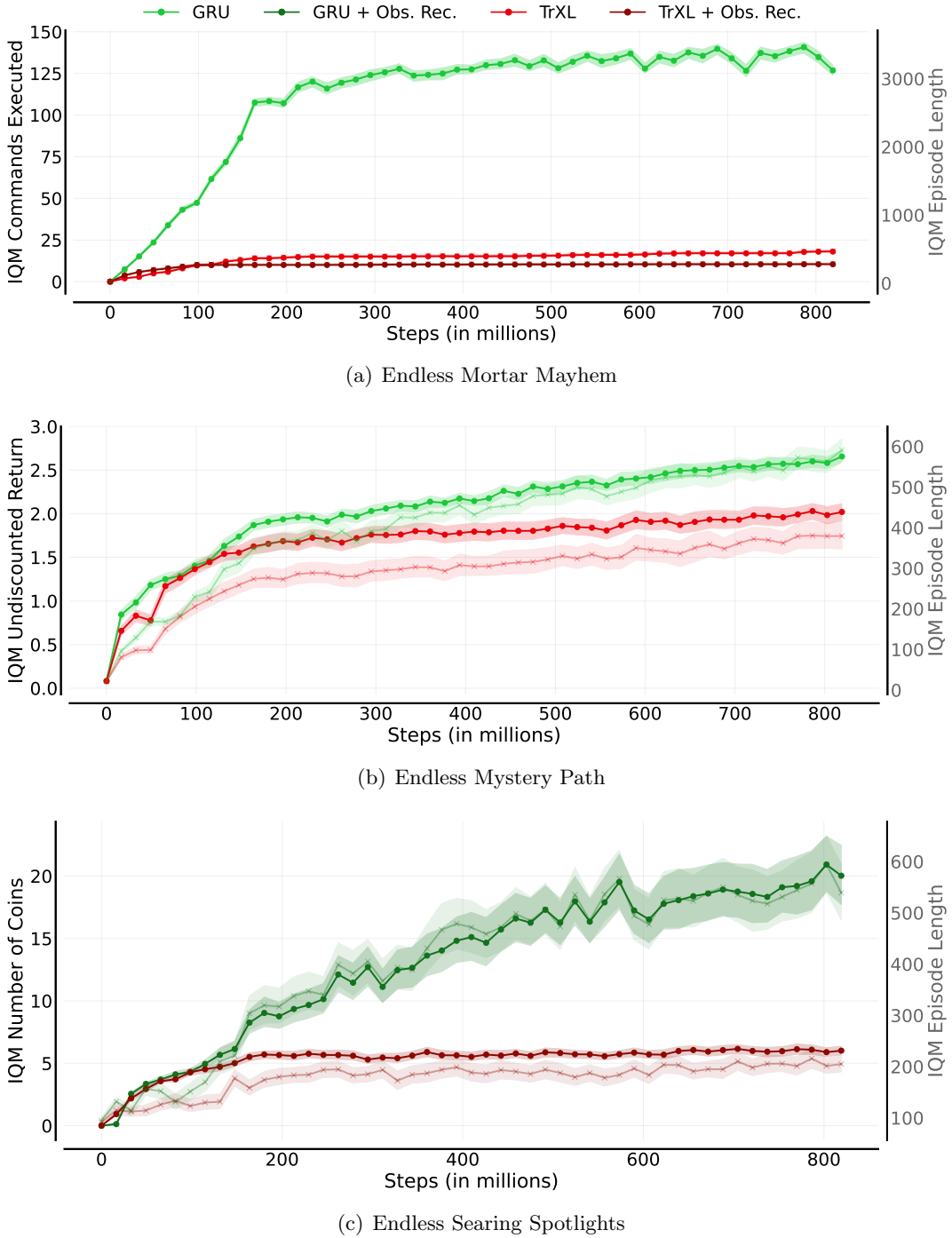


Figure 7: GRU’s consistent superiority over TrXL is revealed in Memory Gym’s endless environments. The less opaque line marked with crosses depicts the interquartile mean (IQM) episode length that refers to the right Y-Axis.

GRU and TrXL emerges in the results of Endless Mortar Mayhem (Figure 7(a)). Within this context, GRU attains an impressive IQM of 125 executed commands using roughly 300 million steps, whereas TrXL only attains an IQM of 18 commands. Furthermore, the incorporation of observation reconstruction exacerbates this performance difference, leading TrXL to a further deterioration, resulting in an IQM of 10. Furthermore, GRU exhibits consistently longer IQM episode lengths, with TrXL achieving an IQM of 288 steps and GRU reaching a peak IQM episode length of 3462 steps.

The outcomes depicted in Figure 7(b) illustrate the results obtained from the Endless Mystery Path environment. In this case, GRU remains more effective than TrXL, although the gap between their performances is narrower compared to Endless Mortar Mayhem. GRU achieves an IQM undiscounted return of 2.65, with TrXL achieving 2.02. Although neither memory approach converges within the allocated training budget of 819 million steps, GRU displays a more pronounced upward trend in performance. In terms of episode length, neither agent achieves lengths as seen in Endless Mortar Mayhem. GRU attains an IQM episode length of 600 steps in Endless Mystery Path, while TrXL reaches up to 400 steps. This divergence can be attributed to the episode’s dynamics, where agents tend to fall off after significant progress, necessitating more steps to regain lost ground and accumulate further rewards.

In Endless Searing Spotlights (Figure 7(c)), GRU is about 3.3 times more effective than TrXL. Both agents utilize the observation reconstruction loss, but TrXL converges to an IQM of 6 collected coins after approximately 200 million steps, while GRU achieves an IQM of about 20 coins, continuing to show an upward trend in its performance. The IQM episode length for TrXL is 200 steps, while GRU achieves a longer IQM episode length of 600 steps.

5.3 Investigating Transformer-XL’s Surprisingly Low Effectiveness

The unexpectedly low performance of TrXL prompts us to examine several hypotheses. Endless Mortar Mayhem, presenting the largest performance gap, serves as our primary environment for these detailed investigations.

5.3.1 INADEQUATE NETWORKS CAPACITY

Our TrXL baseline comprises 2.8 million trainable parameters, while GRU consists of 4.05 million, prompting the question of whether TrXL’s model architecture lacks the necessary capacity. To investigate this, we conducted experiments varying the number of blocks (2, 3, 4), the embedding dimension size (256, 384, 512), and the memory window length (256, 384, 512). None of these adjustments led to closing the performance gap to GRU. Scaling up TrXL also increases its demand for GPU memory. When scaling up multiple architecture details, our implementation and hyperparameters may cause the training to exceed the available 40GB GPU memory of an NVIDIA A100. Workarounds include reducing the batch size or transferring training data between the GPU and CPU, but these options significantly worsen wall-time efficiency. Furthermore, another indication of untapped capacity lies in the amplification of the learning signal, which we elaborate on in the following section.

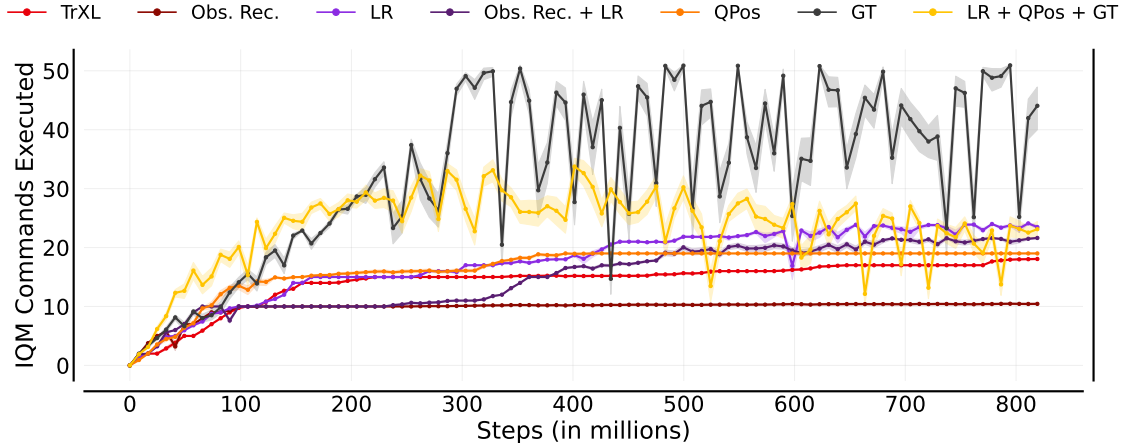


Figure 8: Experiments on Endless Mortar Mayhem with varied TrXL configurations. The learning rate (LR) is adjusted to decay from $2.75e-4$ to $1.0e-4$ over 160 million steps, compared to the previous $1.0e-5$. We also incorporate observation reconstruction (Obs. Rec.) and observe the greatest improvement based on a ground truth estimation head (GT) as sanity check. Another test augments TrXL’s query with relative positional encoding (QPos). The final experiment combines the optimized learning rate, augmented query, and ground truth estimation.

5.3.2 WEAK LEARNING SIGNAL

Figure 8 depicts several additional experiments aimed at amplifying the learning signal. We made a naive adjustment to the learning rate schedule, utilized observation reconstruction, and introduced a ground truth estimation head. This ground truth estimation head is added to the actor-critic model architecture and predicts the target position to move to. Labels are provided by the environment, and the estimates are optimized using the mean-squared error loss. While ground truth information is typically unavailable and considered inappropriate for this benchmark, it serves as a useful sanity check. It helps determine if an additional learning signal is advantageous in this context. When training incorporates ground truth estimation, there is a noticeable improvement in the agent’s policy. Previously, the IQM of completed commands stood at 18; with ground truth estimation, it reaches 50. This outcome implies that the model’s capacity might not be the primary constraint. However, using the ground truth estimation head can lead to instability in training, with the agent’s performance fluctuating between 20 and 50 completed commands after about 300 million steps. During the initial 160 million training steps, the learning rate linearly decays from $2.75e-4$ to $1.0e-5$. By setting the final decayed learning rate to $1.0e-4$, the IQM performance hits 24 commands. Lower performances are observed when adding the observation reconstruction head to either just TrXL or TrXL with the optimized learning rate schedule. In summary, augmenting the learning signal — either by adjusting the learning rate or by incorporating ground truth estimation — leads to more performant policies.

5.3.3 LACK OF TEMPORAL INFORMATION IN THE INITIAL QUERY

The next hypothesis pertains to the initial query of the first TrXL block. This query is constructed solely based on the features extracted from the observation encoders at the current time step, encompassing only minimal temporal information. In contrast, the query of the second block draws from the aggregated outcome of the memory window, thus capturing more substantial temporal information. However, we believe that the initial query could be further enriched with additional information. In Figure 8, one experiment augments the query with absolute positional encoding, providing direct access to the current time step. Despite this enhancement, the agent’s performance only moderately improves, reaching an IQM of 19 completed commands. We also explored embedding the original query with the previous output of the last TrXL block. However, this simple approach did not yield positive results.

5.3.4 HARMFUL OFF-POLICY DATA IN THE EPISODIC MEMORY

Next, it can be discussed whether the combination of PPO and TrXL’s episodic memory pose a threat. PPO is an on-policy algorithm that consumes the training data for a few epochs. Once the second training epoch on the same batch commences, the batch is already considered off-policy. However, PPO’s loss function can mitigate this issue and hence allows for several epochs. But this mitigation is likely limited and we wonder whether this issue is enlarged by the episodic memory. In our current training setup, the agent collects 512 steps of data. If an episode exceeds 512 steps and is still running, the earlier steps from that episode become outdated over multiple epochs. In future work, it needs to be investigated if a stale episodic memory, which is based on off-policy data, hinders training progress. Frequently refreshing hidden states, a process used in the off-policy algorithm R2D2 that relies on recurrence (Kapturowski et al., 2019), is expected to be computationally inefficient.

5.3.5 INDISTINGUISHABLE ABSOLUTE POSITIONAL ENCODING

The final hypothesis concerns a potential limitation of the absolute positional encoding. Without positional encoding, the agent cannot differentiate the time between past observations. As a default, we rely on absolute positional encodings. This encoding always spans across the potential maximum episode length. In the finite environments, the longest range is set to 512, being the sequence length, which is also used in the original transformer (Vaswani et al., 2017). For the endless tasks, this encoding is set up for 2048 steps, an episode duration that is yet unreachable to the TrXL agents.

The original work of TrXL introduces a relative positional encoding (Dai et al., 2019) as a consequence of extended context of lengths. However, when they refer to the absolute positional encoding, they only apply it to the range of the current window. If a window has a length of 4, the positions within the window are always the same (i.e. $[0, 1, 2, 3]$), even though the window moves across the entire sequence. In our case, the absolute positional encoding considers the entire sequence. If the window has progressed in time, the applied positional encoding relies on the current time step (i.e. $[t - 3, t - 2, t - 1, t]$).

Nevertheless, the absolute positional encoding needs to be defined prior training. When scaling it up, the question arises whether the agent’s model is capable of differentiating time steps, because a longer length indicates a more fine-grained sample frequency over the

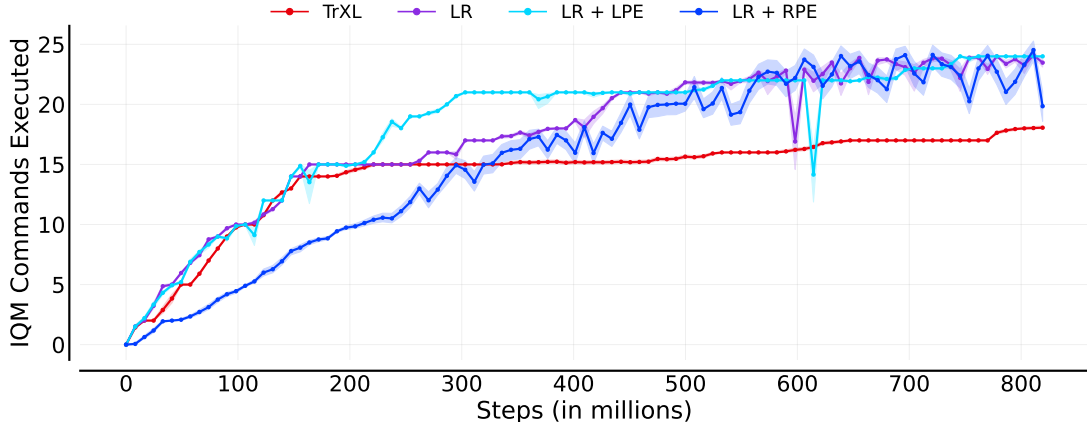


Figure 9: Experiments on Endless Mortar Mayhem with varied positional encoding. The learning rate schedule (LR) is adjusted to decay from $2.75\text{e-}4$ to $1.0\text{e-}4$ over 160 million steps, compared to the previous $1.0\text{e-}5$. The acronym LPE refers to a learned positional encoding, while RPE depicts the relative one.

underlying positional encoding. To test this, we trained a TrXL agent on the finite task of Mortar Mayhem and configured an absolute positional encoding of length 1024 and 2048. Both experiments, which were repeated twice, resulted in an agent that poorly completes only 1 to 2 commands. This demands for questioning the absolute positional encoding in endless tasks. But if the elements of the absolute position encoding of length 2048 are not distinguishable, how do those agents master more than 20 commands in Endless Mortar Mayhem?

If this assumption holds right that the absolute positional encoding is the culprit in our TrXL baseline, leveraging learned or relative positional encodings instead should improve performance. As seen in Figure 9, no notable advancement is accomplished by both variants. We observed two outliers among the 5 runs that utilized relative positional encoding. One underperformed, completing only 13 commands, while the other excelled, finishing more than 60 commands. Since the interquartile mean represents only the central 50% of the data, these outliers are not apparent in the sample efficiency curve. Given this discussion, a more in-depth exploration of positional encoding in this context is advisable.

5.4 Recurrence is not Vulnerable to Spotlight Perturbations

Training recurrent agents in Searing Spotlights with previously established hyperparameters (refer to the last column of Table 4) does not yield a meaningful policy. Despite numerous attempts at hyperparameter tuning, architecture adjustments, and task modifications, Searing Spotlights remained as a puzzle. Even with full observability, where all entities are permanently visible, the performance is catastrophic. These challenges prompted the hypothesis that spotlights might introduce noise, heavily affecting the agent’s policy (Pleines et al., 2023). Support for this theory came from experiments in a simplified BossFight environment (Cobbe et al., 2020), using identical spotlight dynamics as in Searing Spotlights,

Table 1: Results from the ablation study on Searing Spotlights with full observability. Each experiment was run 5 times, though the data sourced directly from the training process deviates from our standard protocol. Every PPO iteration (of 5,000 total) produces a data point that reflects the average over the last 100 episodes. Rows are ordered in descending fashion by the mean success rate. The mean is computed from the top-performing data point, averaged across repetitions, from the specific experiment. Consequently, the time point is represented as a percentage duration. The gradient norm is accumulated over all data points within the given duration.

Experiment	Value		Success Rate		Duration	Gradient Norm	
	New	Old	Mean	Std		Mean	Std
Advantage Norm.	Off	On	1.00	0.00	31%	0.02	0.01
No Memory			0.96	0.11	99%	0.28	0.03
Agent Health Points	5	10	0.79	0.35	99%	0.30	0.02
Transformer-XL			0.69	0.27	99%	0.30	0.03
Agent Speed	3.0	2.5	0.58	0.22	65%	0.33	0.06
Clip Range	0.1	0.2	0.52	0.25	99%	0.27	0.05
Max Episode Length	256	512	0.48	0.27	99%	0.37	0.04
Old Hyperparameters			0.43	0.06	96%	0.38	0.06
Observation Rec.	On	Off	0.39	0.06	96%	0.40	0.04
Max Gradient Norm	0.25	0.5	0.36	0.05	99%	0.24	0.01

suggesting a potential vulnerability of recurrent agents to such perturbation (Pleines et al., 2023).

However, the results presented in Figure 6(g) neglect this hypothesis. This prompted us to conduct an ablation study, beginning with the previous hyperparameters. In this study, only a single hyperparameter or environment option was replaced with the current one at a time. Table 1 presents the results for Searing Spotlights when full observability is ensured. Initially, observation reconstruction was presumed to be the solution. However, the crucial adjustment proved to be the decision to avoid normalizing advantage estimates during optimization. Only the GRU agent, which omits advantage normalization, and the memory-less agent, based entirely on previous hyperparameters, recorded noteworthy success rates of 100% and 96%, respectively.

A salient observation emerges when tracking the gradient norms across the agent models during training. With normalized advantages, the gradient norm is typically more than 12 times greater than when normalization is bypassed. This suggests that during gradient descent, excessively large optimization steps might be taken, resulting in an oscillating behavior that fails to converge to a local minimum. Simultaneously, unnormalized advantages remain at a scale of 2e-4, but post-normalization, the magnitudes stretch beyond 5. Considering that the policy ratio is modulated by these advantage estimates (Schulman et al., 2017), normalization introduces a strikingly different scale than its absence. Standard practice typically normalizes advantages by subtracting the mean and dividing by the standard deviation, often applied at the mini-batch level.

Several comprehensive studies have delved into such nuances of PPO’s implementation (Engstrom et al., 2020; Andrychowicz et al., 2021; Huang et al., 2022b). Among them, only Andrychowicz et al. (2021) turned off advantage normalization and found negligible performance impact. However, their extensive study focused on control tasks with undiscounted returns in the thousands, contrasting Memory Gym’s finite environments where the undiscounted returns do not exceed 2. During hyperparameter optimization, turning off advantage normalization also enhanced performance in Mortar Mayhem and Mystery Path. Given the critical importance of utilizing raw advantages, there remains an opportunity to delve even deeper into PPO to comprehend and refine its essential aspects.

6 Conclusion

In this study, we advanced Memory Gym’s environments to novel endless tasks, tailored to benchmark memory-based Deep Reinforcement Learning algorithms. These tasks feature a mounting challenge similar to the cumulative memory game “I packed my bag”. As the agent’s policy refines, the task dynamically expands, serving as an automatic curriculum. This innovative framework enables a thorough evaluation of memory-based agents, emphasizing their overall effectiveness beyond mere interaction efficiency with the environment.

To foster a more inclusive research landscape, we contributed an open-source PPO baseline powered by Transformer-XL (TrXL). This baseline employs an attention mechanism applied to an episodic memory with a sliding window. When benchmarked against Memory Gym, the TrXL baseline competes head-to-head with another prominent baseline rooted in Gated Recurrent Unit (GRU). Notably, in finite environments, TrXL demonstrates superior effectiveness in Mortar Mayhem and enhanced sample efficiency in Mystery Path. However, in the Searing Spotlights environment, GRU emerges as the more efficient architecture.

Perhaps our most unexpected revelation is the comeback of GRU in the endless environments. GRU surpassed TrXL by large margins, while also being computationally more efficient. Further probing into the Endless Mortar Mayhem environment revealed only marginal improvements for TrXL upon enriching the learning signal.

This prompts future investigations into potential reasons behind TrXL’s limitations, such as the possibility of episodic memory staleness or an initial query lacking temporal awareness. As we move forward, it will be compelling to discern the performance thresholds of other memory mechanisms and DRL algorithms. In addition to examining more attention-based and recurrent architectures, it may be worth exploring structured state space sequence models (Gu et al., 2022), given their recent debut in DRL (Lu et al., 2023).

Acknowledgements

Our sincere appreciation goes to Vincent-Pierre Berges for his enlightening discussions that greatly enriched our work. We also extend our gratitude to Andrew Lampinen for his invaluable insights on utilizing Transformer-XL as episodic memory. Special thanks are due to Günter Rudolph for his unwavering support. This project would not have been possible without the generous computing time provided by the Paderborn Center for Parallel Computing (PC2) and the support from the Linux-HPC-Cluster (LiDO3) at TU Dortmund. We are deeply thankful for all of their contributions.

Appendix A. Environment Parameters

Table 2: Default reset parameters of the finite environments. Parameters marked with an asterisk (*) indicate uniform sampling. Values enclosed in square brackets represent discrete choices, while values in parentheses denote a range from which sampling is performed. For Mortar Mayhem Grid and Mystery Path Grid, the parameters remain the same as its parent, with only the modified ones presented.

Mortar Mayhem		Searing Spotlights	
Parameter	Default	Parameter	Default
Agent Scale	0.25	Max Episode Length	256
Agent Speed	3	Agent Scale	0.25
Arena Size	5	Agent Speed	3
No. Available Commands	9	Agent Always Visible	False
No. Commands*	[10]	Agent Health	5
Command Show Duration*	[3]	Sample Agent Position	True
Command Show Delay*	[1]	Use Exit	True
Execution Duration*	[6]	Exit Scale	0.5
Execution Delay*	[18]	Exit Visible	False
Show Visual Feedback	True	Number of Coins*	[1]
Reward Command Failure	0	Coin Scale	0.375
Reward Command Success	0.1	Coin Always Visible	False
Reward Episode Success	0	No. Initial Spotlight Spawns	4
Mortar Mayhem Grid		Searing Spotlights	
Parameter	Default	Parameter	Default
No. Available Commands	5	No. Spotlight Spawns	30
Execution Duration*	[2]	Spotlight Spawn Interval	30
Execution Delay*	[6]	Spotlight Spawn Decay	0.95
Mystery Path		Searing Spotlights	
Parameter	Default	Parameter	Default
Max Episode Length	512	Spotlight Spawn Threshold	10
Agent Scale	0.25	Spotlight Radius*	(7.5-13.75)
Agent Speed	3	Spotlight Speed*	(0.0025-0.0075)
Cardinal Origin Choice*	[0, 1, 2, 3]	Spotlight Damage	1
Show Origin	False	Light Dim Off Duration	6
Show Goal	False	Light Threshold	255
Show Visual Feedback	True	Show Visual Feedback	True
Reward Goal	1	Show Last Action	True
Reward Fall Off	0	Show Last Positive Reward	True
Reward Path Progress	0.1	Render Background Black	False
Reward Step	0	Hide Checkered Background	False
Mystery Path Grid		Searing Spotlights	
Parameter	Default	Parameter	Default
Max Episode Length	128	Reward Inside Spotlight	0
Reward Path Progress	0	Reward Outside Spotlights	0
		Reward Death	0
		Reward Exit	1
		Reward Coin	0.25
		Reward Max Steps	0

Table 3: Default reset parameters of the endless environments. Parameters marked with an asterisk (*) indicate uniform sampling. Values enclosed in square brackets represent discrete choices, while values in parentheses denote a range from which sampling is performed. If the max episode length is equal or less than zero, episodes will not terminate because of reaching the max episode length.

Endless Mortar Mayhem		Endless Searing Spotlights	
Parameter	Default	Parameter	Default
Max Episode Length	-1	Max Episode Length	-1
Agent Scale	0.25	Agent Scale	0.25
Agent Speed	3	Agent Speed	3
No. Available Commands	9	Agent Always Visible	False
Command Show Duration*	[3]	Agent Health	10
Command Show Delay*	[1]	Sample Agent Position	True
Execution Duration*	[6]	Coin Scale	0.375
Execution Delay*	[18]	Coin Show Duration	6
Show Visual Feedback	True	Coin Always Visible	False
Reward Command Failure	0	Steps per Coin	160
Reward Command Success	0.1	No. Initial Spotlight Spawns	3
Endless Mystery Path		Spotlight Spawn Interval	
Parameter	Default	Spotlight Radius*	(7.5-13.75)
Max Episode Length	-1	Spotlight Speed*	(0.0025-0.0075)
Agent Scale	0.25	Spotlight Damage	1
Agent Speed	3	Light Dim Off Duration	6
Show Origin	False	Light Threshold	255
Show Past Path	True	Show Visual Feedback	True
Show Background	False	Render Background Black	False
Show Stamina	False	Hide Checkered Background	False
Show Visual Feedback	True	Show Last Action	True
Camera Offset Scale	5	Show Last Positive Reward	True
Stamina Level	20	Reward Inside Spotlight	0
Reward Fall Off	0	Reward Outside Spotlights	0
Reward Path Progress	0.1	Reward Death	0
Reward Step	0	Reward Coin	0.25

Appendix B. Hyperparameters

Table 4 presents the hyperparameters utilized in our final experiments unless otherwise specified. The learning rate and entropy coefficient undergo linear decay from their initial to final values. This decay occurs exclusively during the first 10,000 PPO updates (equivalent to 163,840,000 steps). As training progresses beyond this point, the final hyperparameter serves as a lower threshold. Regarding the sequence length and memory window length, they are determined based on the longest possible episode in the finite environments. In the case of endless environments, the so far best sequence length is fixed at 512 for GRU and 256 for TrXL.

Our hyperparameter search was conducted using a customized implementation built upon the optuna tuning framework (Akiba et al., 2019). The objective was to discover

Table 4: Hyperparameters and architectural details used in our final experiments. The “Final” column denotes the selected hyperparameter values, while the “Search Space” column represents additional discrete choices explored during the tuning process. The last column details the old hyperparameters of our previous study (Pleines et al., 2023). For this column alone, empty cells indicate that the values align with those in the “Final” column. T-Fixup is a transformer weight initialization approach by Huang et al. (2020).

Hyperparameter	Final	Search Space			Old
Training Seeds	100000				
Number of Workers	32				
Worker Steps	512				
Batch Size	16384				
Discount Factor Gamma	0.995				0.99
GAE Lamda	0.95				
Optimizer	AdamW				
Epochs	3	2	4		
Number of Mini Batches	8	4			
Advantage Normalization	No	Batch	Mini Batch		Mini Batch
Clip Range Epsilon	0.1	0.2	0.3		0.2
Value Loss Coefficient	0.5	0.25			0.25
Initial Learning Rate	2.75e-4	2.0e-4	3.0e-4	3.5e-4	3.0e-4
Final Learning Rate	1.0e-5				1.0e-4
Initial Entropy Coef.	1.0e-4	1.0e-3	1.0e-2		
Final Entropy Coef.	1.0e-6				1.0e-5
Reconstruction Loss Coef.	0.1	0.5	1.0		n/a
Maximum Gradient Norm	0.25	0.35	0.5	1.0	0.5
Recurrent Neural Network					
Number of Recurrent Layers	1	2			
Embedding Layer	Yes				No
Layer Type	GRU	LSTM			
Residual	False	True			
Sequence Length	512 or max				
Hidden State Size	512	256	384		
Transformer-XL					
Number of TrXL Blocks	3	2	4		
Block Dimension	384	256	512		
Block Weight Initialization	Xavier	Orthogonal	Kaiming	T-Fixup	
Positional Encoding	Relative	None	Learned		
Number of Attention Heads	4	8			
Memory Window Length	256 or max				

a set of hyperparameters that demonstrate strong performance across both our GRU and TrXL baselines and Memory Gym’s environments. Considering limited resources and the computational expense of tuning, we restricted the search space to a limited number of

options. The majority of tuning experiments focused on the finite environments. Therefore, we do not claim to provide optimal hyperparameters.

For each environment, we established individual tuning experiments corresponding to the choices presented in Table 4. Each experiment, or trial, involved a baseline set of hyperparameters that was modified by selecting a single parameter choice from the entire search space. Notably, we did not train permutations of all available choices at this stage. To optimize resource utilization, we implemented optuna’s percentile pruner, which retained the top 25 percentile of trials. Trials that performed below this percentile were pruned, but only after surpassing 2,000 PPO updates as a warm-up phase.

After completing the single experiments, we expanded the hyperparameter search by allowing for permutations sampled using optuna’s Tree-structured Parzen Estimator. It is important to note that individual trials were not repeated, but since tuning was conducted across multiple environments, one could consider them as repetitions in a broader sense.

The batch size is determined by multiplying the number of environment workers by the number of worker steps performed by each worker to gather training data. To efficiently utilize the resources of a system with 32 CPU cores and 40GB VRAM on an nVidia A100 GPU, we chose a batch size of 16,384 samples. However, when scaling up the model, it is possible to exceed the available GPU memory. In such cases, there are two options: reducing the batch size or outsourcing the data to CPU memory. Both of these workarounds come with increased expenses in terms of wall-time.

Appendix C. GTrXL and LSTM Results on the Finite Environments

Figure 10 presents extended results for the finite environments. The performance metrics for TrXL and GRU agents remain consistent with those depicted in Figure 6. However, this figure displays twice as many data points on the x-axis. We include results from agents utilizing Gated Transformer-XL (GTrXL) (Parisotto et al., 2020) and the Long Short-Term Memory (LSTM) (Hochreiter and Schmidhuber, 1997). These models are benchmarked without any hyperparameter tuning. For GTrXL, biases of both 0 and 2 are tested, based on the suggestion by Parisotto et al. (2020) that a larger bias might enhance learning. All additional agents in the Searing Spotlights environment employ the observation reconstruction loss (Obs. Rec.), while it is omitted in the Mystery Path environment.

For Mortar Mayhem (as seen in Figure 10(a)), the LSTM agent settles at 3 commands, whereas the GTrXL agents using observation reconstruction both achieve an IQM of 2 commands. In the Mystery Path results (Figure C), the LSTM agent achieves full success, albeit requiring more samples compared to the GRU and TrXL agents. The GTrXL agent with a bias of 0 reaches a 94% success rate, while the one with a bias of 2 achieves only 81%, challenging the earlier assertion by Parisotto et al. (2020). The confidence interval for these results indicates potential training instability. In the Searing Spotlights environment, the LSTM agent with observation reconstruction is slightly less efficient than its GRU counterpart. However, GTrXL agents, though successful, lag behind TrXL with observation reconstruction.

It is important to note that we avoid making conclusive statements based on these results. This caution stems from the fact that the LSTM and GTrXL baselines are not tuned, and the GTrXL implementation awaits further verification.

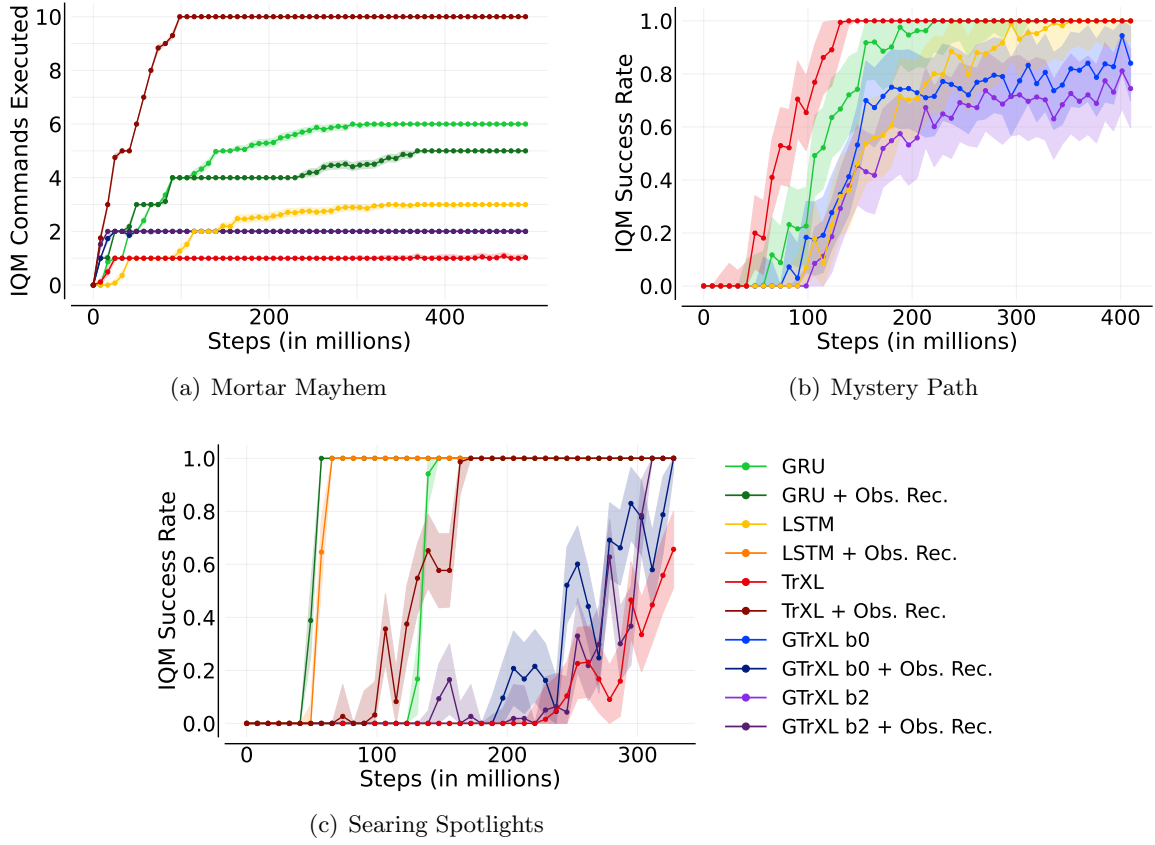


Figure 10: GTrXL and LSTM results on the finite environments.

Appendix D. Wall-Time Efficiency

Reliably reporting the wall-time of all conducted experiments is not feasible due to varying circumstances as varying hardware or different loads of the file system. Therefore, we only provide a selection of measurements on Endless Mortar Mayhem and Mystery Path.

Table 5 presents wall-time efficiency metrics for various agents trained on Endless Mortar Mayhem, utilizing the noctua2 high-performance cluster¹. We leverage 32 CPU cores (AMD Milan 7763), an NVIDIA A100 GPU, and 100GB RAM for one training run. With PyTorch version 2, models can be lazily compiled at training onset, reducing TrXL’s training time by a significant 30%. Previously, plain TrXL training averaged 110 hours, but this has been reduced to 76 hours. Incorporating observation reconstruction adds roughly 3 hours, and with ground truth estimation, it extends to 81 hours. The GRU agents are the most wall-time efficient, completing in approximately 57 hours. Thus, recurrence emerges as the most effective and efficient architecture in both sample and wall-time metrics for the endless environments.

We further take a look at the wall-time of various agents trained on Mystery Path (Figure D). It becomes apparent that TrXL and GRU are quite on par concerning wall-

1. <https://pc2.uni-paderborn.de/de/hpc-services/available-systems/noctua2>

Table 5: Wall-time efficiency metrics for various agents trained on Endless Mortar Mayhem. Agents are arranged from left to right based on increasing mean training duration, measured in hours. Other values are represented in seconds and comprise the time needed for a single update (i.e. one complete iteration of running PPO). The second row indicates if the neural network was compiled before training. Note: TrXL* metrics use 4k initial training data points, while other runs utilize 150k data points covering the full training process.

	GRU	TrXL	TrXL + QPos	TrXL + Obs. Rec.	TrXL + LR + QPos + GT	TrXL*
Compiled	No	Yes	Yes	Yes	Yes	No
Mean	4.11	5.53	5.6	5.76	5.86	7.97
Std	0.35	1.12	1.31	1.1	1.68	0.25
Min	3.6	5.2	5	5.4	5.3	7.6
Median	4.1	5.4	5.5	5.7	5.8	7.9
IQM	4.03	5.48	5.53	5.72	5.82	7.93
Mean Duration	57.08	76.81	77.78	80	81.39	110.69

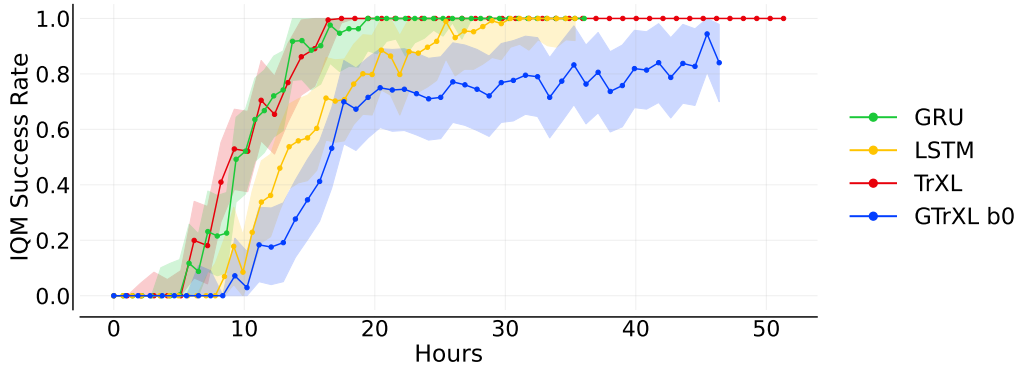


Figure 11: Wall-time

time efficiency, whereas TrXL needs fewer samples as shown in section 5.1. On first sight, it seems surprising that GTrXL is faster than TrXL (Table 6) even though GTrXL is more complex. This is due to the more expensive resets of the environment. Better policies have shorter episodes and thus reset more frequently impairing wall-time. So as GTrXL's and LSTM's policies are inferior, their wall-time is faster. These results were obtained from the LiDo3 high-performance cluster². Each run utilized 32 cores (AMD Epyc 7542), an A100 GPU, and 200GB RAM.

2. <https://lido.itmc.tu-dortmund.de/>

Table 6: Wall-time efficiency metrics for various agents trained on Mytser Path. Agents are arranged from left to right based on increasing mean training duration, measured in hours. Other values are represented in seconds and comprise the time needed for a single update (i.e. one complete iteration of running PPO). The second row indicates if the neural network was compiled before training.

	LSTM	GRU	GTrXL B0	TrXL
Compiled	No	No	Yes	Yes
Mean	5.09	5.19	6.68	7.39
Std	0.22	0.28	0.31	0.24
Min	4.2	4.0	5.8	6.4
Max	7.6	7.0	62.2	11.5
Median	5.1	5.2	6.6	7.4
IQM	5.09	5.18	6.64	7.39
Mean Duration	35.35	36.04	46.4	51.32

References

Rishabh Agarwal, Max Schwarzer, Pablo Samuel Castro, Aaron Courville, and Marc G Bellemare. Deep reinforcement learning at the edge of the statistical precipice. In *Thirty-Fifth Conference on Neural Information Processing Systems*, 2021.

Takuya Akiba, Shotaro Sano, Toshihiko Yanase, Takeru Ohta, and Masanori Koyama. Optuna: A next-generation hyperparameter optimization framework. In Ankur Teredesai, Vipin Kumar, Ying Li, Rómer Rosales, Evinaria Terzi, and George Karypis, editors, *Proceedings of the 25th ACM SIGKDD International Conference on Knowledge Discovery & Data Mining, KDD 2019, Anchorage, AK, USA, August 4-8, 2019*, pages 2623–2631. ACM, 2019. doi: 10.1145/3292500.3330701. URL <https://doi.org/10.1145/3292500.3330701>.

Marcin Andrychowicz, Bowen Baker, Maciek Chociej, Rafal Józefowicz, Bob McGrew, Jakub Pachocki, Arthur Petron, Matthias Plappert, Glenn Powell, Alex Ray, Jonas Schneider, Szymon Sidor, Josh Tobin, Peter Welinder, Lilian Weng, and Wojciech Zaremba. Learning dexterous in-hand manipulation. *Int. J. Robotics Res.*, 39(1), 2020. doi: 10.1177/0278364919887447. URL <https://doi.org/10.1177/0278364919887447>.

Marcin Andrychowicz, Anton Raichuk, Piotr Stańczyk, Manu Orsini, Sertan Girgin, Raphaël Marinier, Leonard Huszenot, Matthieu Geist, Olivier Pietquin, Marcin Michalski, Sylvain Gelly, and Olivier Bachem. What matters for on-policy deep actor-critic methods? a large-scale study. In *International Conference on Learning Representations*, 2021. URL <https://openreview.net/forum?id=nIAxjsniDzg>.

Bowen Baker, Ingmar Kanitscheider, Todor M. Markov, Yi Wu, Glenn Powell, Bob McGrew, and Igor Mordatch. Emergent tool use from multi-agent autocurricula. In *8th International Conference on Learning Representations, ICLR 2020, Addis Ababa, Ethiopia*,

April 26-30, 2020. OpenReview.net, 2020. URL <https://openreview.net/forum?id=SkxpxJBKwS>.

Charles Beattie, Joel Z. Leibo, Denis Teplyashin, Tom Ward, Marcus Wainwright, Heinrich Küttler, Andrew Lefrancq, Simon Green, Víctor Valdés, Amir Sadik, Julian Schrittwieser, Keith Anderson, Sarah York, Max Cant, Adam Cain, Adrian Bolton, Stephen Gaffney, Helen King, Demis Hassabis, Shane Legg, and Stig Petersen. Deepmind lab. *CoRR*, abs/1612.03801, 2016. URL <http://arxiv.org/abs/1612.03801>.

Christopher Berner, Greg Brockman, Brooke Chan, Vicki Cheung, Przemyslaw Debiak, Christy Dennison, David Farhi, Quirin Fischer, Shariq Hashme, Christopher Hesse, Rafal Józefowicz, Scott Gray, Catherine Olsson, Jakub Pachocki, Michael Petrov, Henrique Pondé de Oliveira Pinto, Jonathan Raiman, Tim Salimans, Jeremy Schlatter, Jonas Schneider, Szymon Sidor, Ilya Sutskever, Jie Tang, Filip Wolski, and Susan Zhang. Dota 2 with large scale deep reinforcement learning. *CoRR*, abs/1912.06680, 2019. URL <http://arxiv.org/abs/1912.06680>.

Maxime Chevalier-Boisvert. Miniworld: Minimalistic 3d environment for rl & robotics research. <https://github.com/maximecb/gym-miniworld>, 2018.

Maxime Chevalier-Boisvert, Lucas Willems, and Suman Pal. Minimalistic gridworld environment for openai gym. <https://github.com/maximecb/gym-minigrid>, 2018.

Kyunghyun Cho, Bart van Merriënboer, Çağlar Gülcehre, Dzmitry Bahdanau, Fethi Bougares, Holger Schwenk, and Yoshua Bengio. Learning phrase representations using RNN encoder-decoder for statistical machine translation. In Alessandro Moschitti, Bo Pang, and Walter Daelemans, editors, *Proceedings of the 2014 Conference on Empirical Methods in Natural Language Processing, EMNLP 2014, October 25-29, 2014, Doha, Qatar, A meeting of SIGDAT, a Special Interest Group of the ACL*, pages 1724–1734. ACL, 2014. doi: 10.3115/v1/d14-1179. URL <https://doi.org/10.3115/v1/d14-1179>.

Karl Cobbe, Christopher Hesse, Jacob Hilton, and John Schulman. Leveraging procedural generation to benchmark reinforcement learning. In *Proceedings of the 37th International Conference on Machine Learning, ICML 2020, 13-18 July 2020, Virtual Event*, volume 119 of *Proceedings of Machine Learning Research*, pages 2048–2056. PMLR, 2020. URL <http://proceedings.mlr.press/v119/cobbe20a.html>.

Zihang Dai, Zhilin Yang, Yiming Yang, Jaime G. Carbonell, Quoc Viet Le, and Ruslan Salakhutdinov. Transformer-xl: Attentive language models beyond a fixed-length context. In Anna Korhonen, David R. Traum, and Lluís Màrquez, editors, *Proceedings of the 57th Conference of the Association for Computational Linguistics, ACL 2019, Florence, Italy, July 28- August 2, 2019, Volume 1: Long Papers*, pages 2978–2988. Association for Computational Linguistics, 2019. doi: 10.18653/v1/p19-1285. URL <https://doi.org/10.18653/v1/p19-1285>.

Jonas Degrave, Federico Felici, Jonas Buchli, Michael Neunert, Brendan Tracey, Francesco Carpanese, Timo Ewalds, Roland Hafner, Abbas Abdolmaleki, Diego de las Casas, Craig

Donner, Leslie Fritz, Cristian Galperti, Andrea Huber, James Keeling, Maria Tsimpoukelli, Jackie Kay, Antoine Merle, Jean-Marc Moret, Seb Noury, Federico Pesamosca, David Pfau, Olivier Sauter, Cristian Sommariva, Stefano Coda, Basil Duval, Ambrogio Fasoli, Pushmeet Kohli, Koray Kavukcuoglu, Demis Hassabis, and Martin Riedmiller. Magnetic control of tokamak plasmas through deep reinforcement learning. *Nature*, 602(7897):414–419, Feb 2022. ISSN 1476-4687. doi: 10.1038/s41586-021-04301-9. URL <https://doi.org/10.1038/s41586-021-04301-9>.

Rudi D’Hooge and Peter P De Deyn. Applications of the morris water maze in the study of learning and memory. *Brain research reviews*, 36(1):60–90, 2001.

Logan Engstrom, Andrew Ilyas, Shibani Santurkar, Dimitris Tsipras, Firdaus Janoos, Larry Rudolph, and Aleksander Madry. Implementation matters in deep RL: A case study on PPO and TRPO. In *8th International Conference on Learning Representations, ICLR 2020, Addis Ababa, Ethiopia, April 26-30, 2020*. OpenReview.net, 2020. URL <https://openreview.net/forum?id=r1etN1rtPB>.

Lasse Espeholt, Hubert Soyer, Rémi Munos, Karen Simonyan, Volodymyr Mnih, Tom Ward, Yotam Doron, Vlad Firoiu, Tim Harley, Iain Dunning, Shane Legg, and Koray Kavukcuoglu. IMPALA: scalable distributed deep-rl with importance weighted actor-learner architectures. In Jennifer G. Dy and Andreas Krause, editors, *Proceedings of the 35th International Conference on Machine Learning, ICML 2018, Stockholmsmässan, Stockholm, Sweden, July 10-15, 2018*, volume 80 of *Proceedings of Machine Learning Research*, pages 1406–1415. PMLR, 2018. URL <http://proceedings.mlr.press/v80/espeholt18a.html>.

Linxi Fan, Guanzhi Wang, Yunfan Jiang, Ajay Mandlekar, Yuncong Yang, Haoyi Zhu, Andrew Tang, De-An Huang, Yuke Zhu, and Anima Anandkumar. Mine dojo: Building open-ended embodied agents with internet-scale knowledge. In *NeurIPS*, 2022. URL http://papers.nips.cc/paper_files/paper/2022/hash/74a67268c5cc5910f64938cac4526a90-Abstract-Datasets_and_Benchmarks.html.

Meire Fortunato, Melissa Tan, Ryan Faulkner, Steven Hansen, Adrià Puigdomènech Badia, Gavin Buttimore, Charles Deck, Joel Z Leibo, and Charles Blundell. Generalization of reinforcement learners with working and episodic memory. In *Advances in Neural Information Processing Systems*, pages 12448–12457, 2019.

Albert Gu, Karan Goel, and Christopher Ré. Efficiently modeling long sequences with structured state spaces. In *The Tenth International Conference on Learning Representations, ICLR 2022, Virtual Event, April 25-29, 2022*. OpenReview.net, 2022. URL <https://openreview.net/forum?id=uYLfOz1vlAC>.

Matthew J. Hausknecht and Peter Stone. Deep recurrent q-learning for partially observable mdps. In *2015 AAAI Fall Symposia, Arlington, Virginia, USA, November 12-14, 2015*, pages 29–37. AAAI Press, 2015. URL <http://www.aaai.org/ocs/index.php/FSS/FSS15/paper/view/11673>.

Nicolas Heess, Jonathan J. Hunt, Timothy P. Lillicrap, and David Silver. Memory-based control with recurrent neural networks. *CoRR*, abs/1512.04455, 2015. URL <http://arxiv.org/abs/1512.04455>.

Felix Hill, Olivier Tieleman, Tamara von Glehn, Nathaniel Wong, Hamza Merzic, and Stephen Clark. Grounded language learning fast and slow. In *9th International Conference on Learning Representations, ICLR 2021, Virtual Event, Austria, May 3-7, 2021*. OpenReview.net, 2021. URL https://openreview.net/forum?id=wpSWuz_hyqA.

Sepp Hochreiter and Jürgen Schmidhuber. Long short-term memory. *Neural Comput.*, 9(8):1735–1780, 1997. doi: 10.1162/neco.1997.9.8.1735. URL <https://doi.org/10.1162/neco.1997.9.8.1735>.

Shengyi Huang, Rousslan Fernand Julien Dossa, Antonin Raffin, Anssi Kanervisto, and Weixun Wang. The 37 implementation details of proximal policy optimization. ICLR Blog Track, 2022a. URL <https://iclr-blog-track.github.io/2022/03/25/ppo-implementation-details/>.

Shengyi Huang, Rousslan Fernand Julien Dossa, Antonin Raffin, Anssi Kanervisto, and Weixun Wang. The 37 implementation details of proximal policy optimization. In *ICLR Blog Track*, 2022b. URL <https://iclr-blog-track.github.io/2022/03/25/ppo-implementation-details/>. Accessed: 2023-09-18.

Xiao Shi Huang, Felipe Pérez, Jimmy Ba, and Maksims Volkovs. Improving transformer optimization through better initialization. In *Proceedings of the 37th International Conference on Machine Learning, ICML 2020, 13-18 July 2020, Virtual Event*, volume 119 of *Proceedings of Machine Learning Research*, pages 4475–4483. PMLR, 2020. URL <http://proceedings.mlr.press/v119/huang20f.html>.

Max Jaderberg, Wojciech M. Czarnecki, Iain Dunning, Luke Marris, Guy Lever, Antonio García Castañeda, Charles Beattie, Neil C. Rabinowitz, Ari S. Morcos, Avraham Ruderman, Nicolas Sonnerat, Tim Green, Louise Deason, Joel Z. Leibo, David Silver, Demis Hassabis, Koray Kavukcuoglu, and Thore Graepel. Human-level performance in first-person multiplayer games with population-based deep reinforcement learning. *CoRR*, abs/1807.01281, 2018. URL <http://arxiv.org/abs/1807.01281>.

Steven Kapturowski, Georg Ostrovski, Will Dabney, John Quan, and Remi Munos. Recurrent experience replay in distributed reinforcement learning. In *International Conference on Learning Representations*, 2019. URL <https://openreview.net/forum?id=r1lyTjAqYX>.

Andrew Kyle Lampinen, Stephanie C.Y. Chan, Andrea Banino, and Felix Hill. Towards mental time travel: a hierarchical memory for reinforcement learning agents. In A. Beygelzimer, Y. Dauphin, P. Liang, and J. Wortman Vaughan, editors, *Advances in Neural Information Processing Systems*, 2021. URL https://openreview.net/forum?id=wfiVgITyCC_.

Joel Z. Leibo, Cyprien de Masson d’Autume, Daniel Zoran, David Amos, Charles Beattie, Keith Anderson, Antonio García Castañeda, Manuel Sanchez, Simon Green, Audrunas

Gruslys, Shane Legg, Demis Hassabis, and Matthew M. Botvinick. Psychlab: A psychology laboratory for deep reinforcement learning agents. *CoRR*, abs/1801.08116, 2018. URL <http://arxiv.org/abs/1801.08116>.

Chris Lu, Yannick Schroecker, Albert Gu, Emilio Parisotto, Jakob Nicolaus Foerster, Satinder Singh, and Feryal Behbahani. Structured state space models for in-context reinforcement learning. In *ICML Workshop on New Frontiers in Learning, Control, and Dynamical Systems*, 2023. URL <https://openreview.net/forum?id=CKPTz21e6k>.

Lingheng Meng, Rob Gorbet, and Dana Kulic. Memory-based deep reinforcement learning for pomdps. In *IEEE/RSJ International Conference on Intelligent Robots and Systems, IROS 2021, Prague, Czech Republic, September 27 - Oct. 1, 2021*, pages 5619–5626. IEEE, 2021. doi: 10.1109/IROS51168.2021.9636140. URL <https://doi.org/10.1109/IROS51168.2021.9636140>.

Volodymyr Mnih, Koray Kavukcuoglu, David Silver, Andrei A. Rusu, Joel Veness, Marc G. Bellemare, Alex Graves, Martin A. Riedmiller, Andreas Fidjeland, Georg Ostrovski, Stig Petersen, Charles Beattie, Amir Sadik, Ioannis Antonoglou, Helen King, Dharshan Kumaran, Daan Wierstra, Shane Legg, and Demis Hassabis. Human-level control through deep reinforcement learning. *Nat.*, 518(7540):529–533, 2015. doi: 10.1038/nature14236. URL <https://doi.org/10.1038/nature14236>.

Volodymyr Mnih, Adrià Puigdomènech Badia, Mehdi Mirza, Alex Graves, Timothy P. Lillicrap, Tim Harley, David Silver, and Koray Kavukcuoglu. Asynchronous methods for deep reinforcement learning. In Maria-Florina Balcan and Kilian Q. Weinberger, editors, *Proceedings of the 33nd International Conference on Machine Learning, ICML 2016, New York City, NY, USA, June 19-24, 2016*, volume 48 of *JMLR Workshop and Conference Proceedings*, pages 1928–1937. JMLR.org, 2016. URL <http://proceedings.mlr.press/v48/mnih16.html>.

Steven Morad, Ryan Kortvelesy, Matteo Bettini, Stephan Liwicki, and Amanda Prorok. POPGym: Benchmarking partially observable reinforcement learning. In *The Eleventh International Conference on Learning Representations*, 2023. URL <https://openreview.net/forum?id=chDrutUTsOK>.

Fabian Paischer, Thomas Adler, Vihang P. Patil, Angela Bitto-Nemling, Markus Holzleitner, Sebastian Lehner, Hamid Eghbal-Zadeh, and Sepp Hochreiter. History compression via language models in reinforcement learning. In Kamalika Chaudhuri, Stefanie Jegelka, Le Song, Csaba Szepesvári, Gang Niu, and Sivan Sabato, editors, *International Conference on Machine Learning, ICML 2022, 17-23 July 2022, Baltimore, Maryland, USA*, volume 162 of *Proceedings of Machine Learning Research*, pages 17156–17185. PMLR, 2022a. URL <https://proceedings.mlr.press/v162/paischer22a.html>.

Fabian Paischer, Thomas Adler, Andreas Radler, Markus Hofmarcher, and Sepp Hochreiter. Toward semantic history compression for reinforcement learning. In *Second Workshop on Language and Reinforcement Learning*, 2022b. URL <https://openreview.net/forum?id=97C6klf5shp>.

Emilio Parisotto and Ruslan Salakhutdinov. Efficient transformers in reinforcement learning using actor-learner distillation. In *9th International Conference on Learning Representations, ICLR 2021, Virtual Event, Austria, May 3-7, 2021*. OpenReview.net, 2021. URL https://openreview.net/forum?id=uR9La0_QxF.

Emilio Parisotto, H. Francis Song, Jack W. Rae, Razvan Pascanu, Caglar Gülcöhre, Siddhant M. Jayakumar, Max Jaderberg, Raphaël Lopez Kaufman, Aidan Clark, Séb Noury, Matthew M. Botvinick, Nicolas Heess, and Raia Hadsell. Stabilizing transformers for reinforcement learning. In *Proceedings of the 37th International Conference on Machine Learning, ICML 2020, 13-18 July 2020, Virtual Event*, volume 119 of *Proceedings of Machine Learning Research*, pages 7487–7498. PMLR, 2020. URL <http://proceedings.mlr.press/v119/parisotto20a.html>.

Jurgis Pašukonis, Timothy P Lillicrap, and Danijar Hafner. Evaluating long-term memory in 3d mazes. In *The Eleventh International Conference on Learning Representations*, 2023. URL <https://openreview.net/forum?id=yHLvI1E9RGN>.

Marco Pleines, Matthias Pallasch, Frank Zimmer, and Mike Preuss. Memory gym: Partially observable challenges to memory-based agents. In *The Eleventh International Conference on Learning Representations*, 2023. URL <https://openreview.net/forum?id=jHc8dCx6DDr>.

David E. Rumelhart, Geoffrey E. Hinton, and Ronald J. Williams. Learning representations by back-propagating errors. *Nature*, 323(6088):533–536, 1986. ISSN 1476-4687. doi: 10.1038/323533a0. URL <https://doi.org/10.1038/323533a0>.

John Schulman, Philipp Moritz, Sergey Levine, Michael I. Jordan, and Pieter Abbeel. High-dimensional continuous control using generalized advantage estimation. In Yoshua Bengio and Yann LeCun, editors, *4th International Conference on Learning Representations, ICLR 2016, San Juan, Puerto Rico, May 2-4, 2016, Conference Track Proceedings*, 2016. URL <http://arxiv.org/abs/1506.02438>.

John Schulman, Filip Wolski, Prafulla Dhariwal, Alec Radford, and Oleg Klimov. Proximal policy optimization algorithms. *arXiv:1707.06347*, 2017.

Wenling Shang, Xiaofei Wang, Aravind Srinivas, Aravind Rajeswaran, Yang Gao, Pieter Abbeel, and Michael Laskin. Reinforcement learning with latent flow. In Marc’Aurelio Ranzato, Alina Beygelzimer, Yann N. Dauphin, Percy Liang, and Jennifer Wortman Vaughan, editors, *Advances in Neural Information Processing Systems 34: Annual Conference on Neural Information Processing Systems 2021, NeurIPS 2021, December 6-14, 2021, virtual*, pages 22171–22183, 2021. URL <https://proceedings.neurips.cc/paper/2021/hash/ba3c5fe1d6d6708b5bffaeb6942b7e04-Abstract.html>.

Ashish Vaswani, Noam Shazeer, Niki Parmar, Jakob Uszkoreit, Llion Jones, Aidan N. Gomez, Łukasz Kaiser, and Illia Polosukhin. Attention is all you need. In Isabelle Guyon, Ulrike von Luxburg, Samy Bengio, Hanna M. Wallach, Rob Fergus, S. V. N. Vishwanathan, and Roman Garnett, editors, *Advances in Neural Information Processing Systems 30: Annual Conference on Neural Information Processing Systems 2017, December 4-9, 2017, Long Beach, CA, USA*,

pages 5998–6008, 2017. URL <https://proceedings.neurips.cc/paper/2017/hash/3f5ee243547dee91fdb053c1c4a845aa-Abstract.html>.

Oriol Vinyals, Igor Babuschkin, Wojciech M. Czarnecki, Michaël Mathieu, Andrew Dudzik, Junyoung Chung, David H. Choi, Richard Powell, Timo Ewalds, Petko Georgiev, Junhyuk Oh, Dan Horgan, Manuel Kroiss, Ivo Danihelka, Aja Huang, Laurent Sifre, Trevor Cai, John P. Agapiou, Max Jaderberg, Alexander Sasha Vezhnevets, Rémi Leblond, Tobias Pohlen, Valentin Dalibard, David Budden, Yury Sulsky, James Molloy, Tom Le Paine, Çaglar Gülcöhre, Ziyu Wang, Tobias Pfaff, Yuhuai Wu, Roman Ring, Dani Yogatama, Dario Wünsch, Katrina McKinney, Oliver Smith, Tom Schaul, Timothy P. Lillicrap, Koray Kavukcuoglu, Demis Hassabis, Chris Apps, and David Silver. Grandmaster level in starcraft II using multi-agent reinforcement learning. *Nat.*, 575(7782):350–354, 2019. doi: 10.1038/s41586-019-1724-z. URL <https://doi.org/10.1038/s41586-019-1724-z>.

Rui Wang, Joel Lehman, Aditya Rawal, Jiale Zhi, Yulun Li, Jeffrey Clune, and Kenneth O. Stanley. Enhanced POET: open-ended reinforcement learning through unbounded invention of learning challenges and their solutions. In *Proceedings of the 37th International Conference on Machine Learning, ICML 2020, 13-18 July 2020, Virtual Event*, volume 119 of *Proceedings of Machine Learning Research*, pages 9940–9951. PMLR, 2020. URL <http://proceedings.mlr.press/v119/wang201.html>.

Daan Wierstra, Alexander Förster, Jan Peters, and Jürgen Schmidhuber. Solving deep memory pomdps with recurrent policy gradients. In Joaquim Marques de Sá, Luís A. Alexandre, Włodzisław Duch, and Danilo P. Mandic, editors, *Artificial Neural Networks - ICANN 2007, 17th International Conference, Porto, Portugal, September 9-13, 2007, Proceedings, Part I*, volume 4668 of *Lecture Notes in Computer Science*, pages 697–706. Springer, 2007. doi: 10.1007/978-3-540-74690-4_71. URL https://doi.org/10.1007/978-3-540-74690-4_71.

Marek Wydmuch, Michał Kempka, and Wojciech Jaśkowski. Vizdoom competitions: Playing doom from pixels. *IEEE Transactions on Games*, 2018.